Thermochimica Acta 665 (2018) 53–59

Contents lists available at ScienceDirect

Thermochimica Acta

journal homepage: www.elsevier.com/locate/tca

Deconvolution of overlapping peaks from differential scanning calorimetry analysis for multi-phase NiTi alloys

A. Michael[a,*], Y.N. Zhou[a], M. Yavuz[a], M.I. Khan[b]

[a] Centre for Advanced Materials Joining (CAMJ), Department of Mechanical and Mechatronics Engineering, University of Waterloo, 200 University Avenue West, Waterloo, ON, N2L 3G1, Canada
[b] Smarter Alloys Inc., 75 Bathurst Drive, Waterloo, ON, N2V1N2, Canada

ARTICLE INFO

Keywords:
Nickel-titanium
NiTi
Shape memory alloy (SMA)
Differential scanning calorimetry (DSC)
Deconvolution
Multi-phase
Multiple memory

ABSTRACT

An adaptive function capable of fitting the curve of Differential Scanning Calorimetry (DSC) data for any NiTi phase transformation peak has been developed. A novel methodology was applied in conjunction with this new equation, allowing for the deconvolution of multiple overlapping NiTi phase transformation peaks. Characteristic transformation properties determine by this methodology closely matched those ascertainable by current analysis techniques. This novel analysis technique allows for better determination of characteristic properties of complex NiTi materials with overlapping phase transformations or multiple embedded memories.

1. Introduction

Shape memory alloys (SMAs) exhibit the advantageous properties of pseudoelasticity (PE) and shape memory effect (SME). These special properties are a result of their crystallographic reversible martensitic transformation, which can be induced by either temperature or stress. For NiTi, the material transitions from austenite (B2) to martensite (B19') directly or through a multiple-stage transition from austenite to R-phase to martensite. Initial characterization of an SMA begins with determining the characteristic transformation temperatures, usually by differential scanning calorimetry (DSC) [1–5], electrical resistivity scanning (ERS) [5–7] or bend and free recovery (BFR) [8–10]. The BFR method is only capable of showing transformation temperatures upon heating; however, DSC and ESR can also ascertain the transformation temperatures for heating and/or cooling. In addition, DSC analysis can also determine the enthalpy and entropy changes during phase transformation [1,11].

When the NiTi SMA goes through a multi-stage phase transformation, it is possible for the austenite to R-phase transition and the R-phase to martensite transition to have overlapping temperature ranges [12]. This phenomenon makes it difficult to determine when the first transition actually ends or when the second one actually starts. It also makes it difficult to determine what the latent heats of transformation are for each individual transformation [13]. In some cases, the transitions coincide well enough that they are treated as a single transformation for simplification reasons [1]. Deconvoluting overlapping peaks is a common occurrence for many spectral analysis techniques. However, these techniques are typically looking for specific elements or compounds that behave in a predictable manor. The maximum peak height will be in a known location (plus or minus a known amount) and the peak height-to-width ratio will also be known in advance. This foreknowledge of the exact shape and location of the peak makes isolation of an individual peak from a group of overlapping peaks relatively easy. Modelling and deconvolution of DSC peaks, while more complex than spectral analysis, has also been performed on generic DSC data; however, this technique requires some knowledge of the reaction kinetics that will occur or the mathematics becomes extremely complicated [14]. Simpler methods rely on standard distribution models; however, these methods may not be suitable for curve fitting NiTi transformation peaks. The transformation kinetics for NiTi are not easily predetermined and the peak shapes are non-uniform and vary greatly. The thermomechanical history [15–18] as well as changes in composition [18–20] will result in different shapes and locations for the transformation peaks. The numerous combinations of composition, grain size, precipitate size/density, etc. make developing a complete correlation between microstructure and transformation kinetics an unfathomable undertaking. This is further complicated when multiple compositions are contained in a monolithic material [21].

This study sets out to develop an adaptive function that can be fit to any shape of peak for NiTi DSC data. An algorithm will be put forth to separate overlapping DSC peaks and determine the individual peak characteristics. This research will help to better understand the

* Corresponding author.
E-mail address: a2michae@uwaterloo.ca (A. Michael).

https://doi.org/10.1016/j.tca.2018.05.014
Received 16 August 2017; Received in revised form 15 May 2018; Accepted 16 May 2018
Available online 17 May 2018
0040-6031/

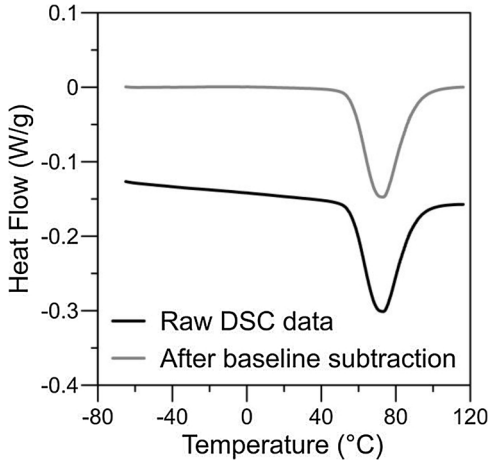

Fig. 1. Depiction of a NiTi DSC transformation peak before and after a baseline subtraction is performed.

fundamental thermodynamic properties of some of the more complex NiTi SMAs with multi-stage phase transformations.

2. Experimental section

2.1. Material selection

A NiTi wire from Furukawa Electric Co. LTD. with a diameter of 700 µm, a composition of 50.8 at.% Ni and pseudoelastic properties at room temperature was used for this study. Some of this material was annealed at 600 °C for 1 h, which resulted in a narrower DSC peak. It has been shown that extended annealing increases the relative intensity of the transformation peak [13], which is due in part to an increase in the homogeneity of the microstructure [22]. This material will be referred to as annealed wire (AW) for the remainder of this study. Some of the base material wire sample was processed with a laser to modify and control the wire composition, in line with previous studies [23,24]. The laser used for processing wires was a Miyachi Unitek LW50A pulsed Nd:YAG laser with a wavelength of 1064 nm. These wires will be referred to as processed wire (i.e. PW1, PW2, PW3, PW4) henceforth. Additionally, one of the laser processed wires went through a cold-working and heat treatment regime, in line with previous studies [24,25] in order to create a microstructure that facilitated an intermediate R-phase transformation [25,26]. This material will be referred to as treated processed wire (TPW).

A NiTi sheet from Memry with a thickness of 2.5 mm, a composition of 50.8 at.% Ni and pseudoelastic properties at room temperature was also used for this study. This material will be referred to as base material sheet (BMS) for the remainder of this study. One of the sheet samples was processed with a laser to modify and control the composition in part of the sheet. The laser used for processing the sheets was a Miyachi Unitek LW15 pulsed Nd:YAG laser with a wavelength of 1064 nm. This material will be referred to as processed sheet (PS).

2.2. Material characterization

A TA Discovery DSC equipped with a refrigerator cooling system was used for Differential Scanning Calorimetry (DSC) analysis. The material was first thermally cycled from room temperature to 120 °C to −75 °C at a heating/cooling rate of 20 °C/min. This pre-cycling was done to remove any effects of internal mechanical stresses that may have been generated by laser processing. Then, data was recorded from −75 °C to 120 °C using a controlled heating/cooling rate of 10 °C/min, per the ASTM F2004-05 (2010) standard [3]. An Olympus BX51M was used for optical microscopy of sample cross-sections.

3. Curve fitting to a single NiTi transformation peak

Prior to curve fitting the data, a simple baseline subtraction if performed. Regression analysis is done on several data points not contained within the transformation peak. The function that best fits these data points is subtracted from the data, as shown in Fig. 1. The baseline subtraction is performed first to simplify the process of curve fitting the NiTi DSC phase transformation peak(s).

Due to the variability of peak shapes, an adaptive function was necessary. The function developed for this study was:

$$q^* = \frac{k}{1 + \left(\frac{abs(p-T)}{\sigma}\right)^n + \left(\frac{abs(p-T)}{\sigma}\right)^m} \quad (1)$$

where k is a scaling factor, p is the peak temperature, and σ is the peak spread at 1/3 height. The exponent n controls the curvature of the function and the base of the peak and the exponent m controls the curvature at the crest of the peak. At this time, the equation is a purely a mathematical expression that best represents the transformation curve and currently does not have any physical relationship to the actual phase transformation kinetics. A program was created in *Matlab*™ to solve for n and m. Due to the skewness of the transformation peak, the function is split into two piecewise functions, one for the onset (Eq. (2)) and one for the endset (Eq. (3)) of the transformation:

$$if\ T \le p,\ \ q^* = \frac{k_1}{1 + \left(\frac{p-T}{\sigma_1}\right)^{n_1} + \left(\frac{p-T}{\sigma_1}\right)^{m_1}} \quad (2)$$

$$if\ T > p,\ \ q^* = \frac{k_2}{1 + \left(\frac{T-p}{\sigma_2}\right)^{n_2} + \left(\frac{T-p}{\sigma_2}\right)^{m_2}} \quad (3)$$

Each equation is solved independently to best fit the skewness of the transformation peak. This function allows for curve fitting of any peak shape, regardless of the height to width ratio or the asymmetry of the peak.

Fig. 2 shows how well the new function fits the individual peaks of two different NiTi samples. Also a comparison with a standard Fraser-Suzuki asymmetric Gaussian model and a Cauchy model are shown. The DSC peak of the AW sample has an apparent skewed distribution, with the onset be more gradual and the endset being more abrupt. This is born out in the parameters used to model the peak. The σ value for the onset is larger than for the endset, indicating a skewed distribution. Additionally, the n and m values for the onset are smaller than the endset values, indicating a steeper curve for the endset. The residual error for this new method is significantly lower than the two standard methods examine. The Fraser-Suzuki method can account for the skewness relatively well, but it cannot account for the base of the peak being relatively wide. The Cauchy method does well matching the top to bottom distribution, but it is unable to fit the large asymmetry present in this peak.

The asymmetry of the PW1 sample is less apparent. Both the onset and endset have comparable σ values because the peak is more evenly distributed; however, the n and m values of the onset are larger than then endset because the endset has a more gradual transition. The peak for PW1 is broader than the peak for AW, which is reflected by much larger σ values for PW1 than AW. The Fraser-Suzuki method does appear to match the PW1 curve well, however it still has a larger residual error than the newly proposed method. Overall, the new method does a much better job at curve fitting the data, as the standard methods do not have enough parameters to account for to non-standard shape of the NiTi transformation peaks. All of the relevant parameters for the new model are shown in Table 1. A comparison of the characteristic peak values is shown in Fig. 2.

Furthermore, calculating the austenite start (As) and austenite finish (Af) temperatures becomes a simple matter. These characteristic temperatures are determined by the intersection of the peak baseline and a

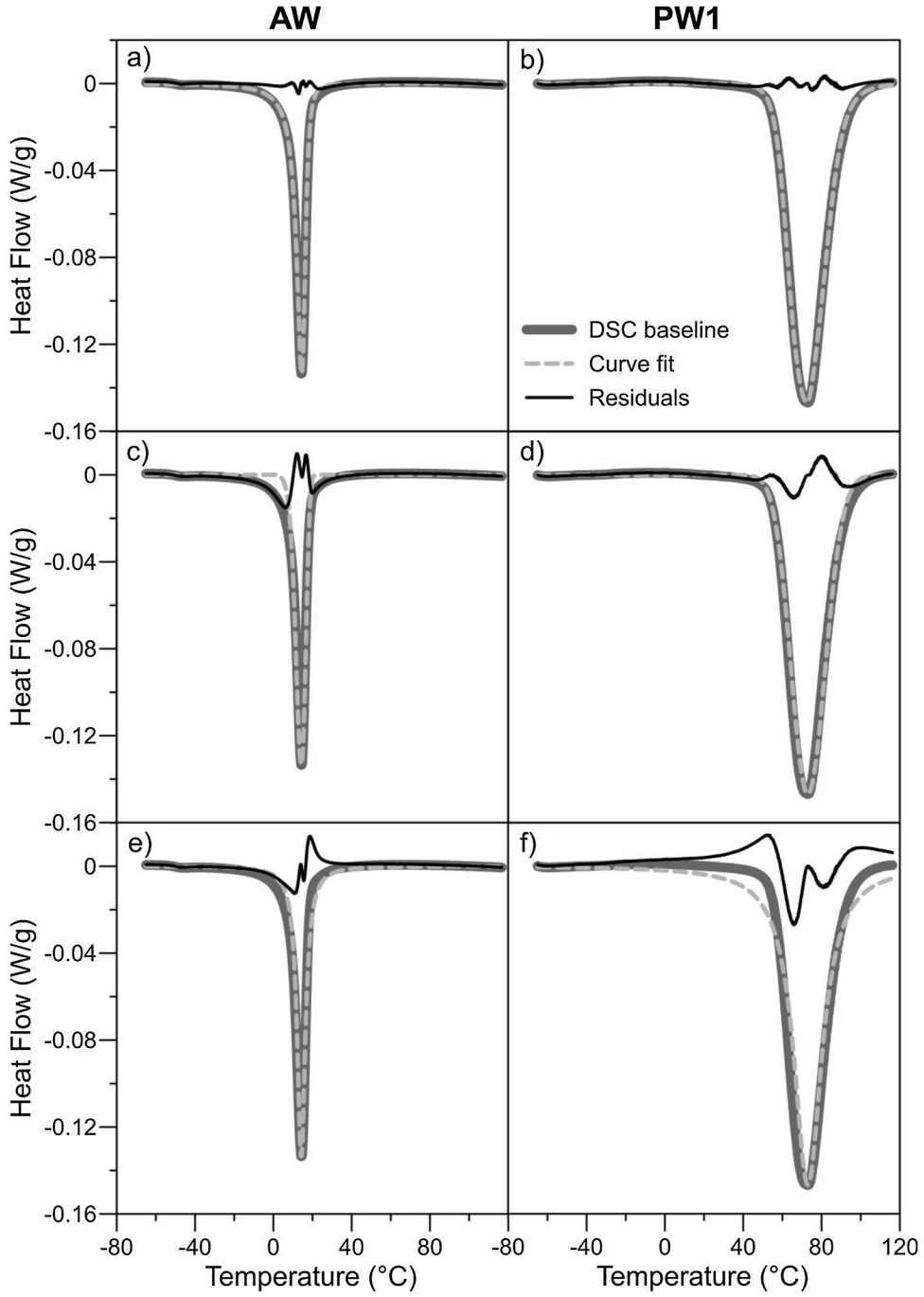

Fig. 2. Depictions of curves fitting the DSC data for the AW and PW1 samples using a–b) the proposed new model, c–d) a Fraser–Suzuki asymmetric Gaussian model and e–f) a Cauchy model.

Table 1
List of function parameters and transformation characteristics for single peak NiTi samples using the new model.

	p	Onset				Endset			
		k	σ	n	m	k	σ	n	m
AW	14.261	−0.133	4.457	2.1	1.4	−0.133	3.093	3.3	2.4
PW1	73.034	−0.147	13.131	6.1	2.3	−0.147	13.101	4.4	1.5

tangent line running through the inflection point [3]. This inflection point is where the second derivative of the equation is equal to zero. The As and Af temperatures for the single peaks were determined in this manner and compared with analysis performed using Trios software v3.2 (see Table 2), which is available from TA Instruments. The two methods showed comparable characteristic temperatures for both samples. These results validate this method as a means for fitting the DSC phase transformation peak and properly characterizing any NiTi sample with a single-phase transition.

4. Deconvoluting overlapping NiTi transformation peaks

4.1. Multiple phase transformations

Many NiTi shape memory alloys have an intermediary R-phase transformation that reduces the amount of kinetic energy required to

Table 2
Comparison between new method and commercially available software for peak characteristic values.

	Derivative Method				Trios Software			
	As (°C)	Ap (°C)	Af (°C)	Area J/g	As (°C)	Ap (°C)	Af (°C)	Area J/g
AW	8.9	14.3	18.2	12.7	8.9	14.3	18.3	13.1
PW1	55.9	73.0	91.4	20.0	55.7	73.0	89.8	20.2

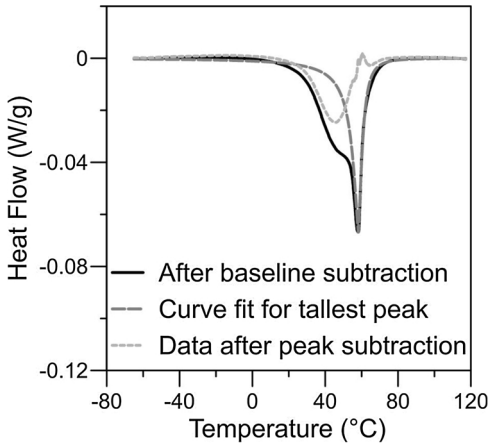

Fig. 3. Depiction of first iteration of curve fitting the taller peak and subtracting it from the data.

transition from martensite to austenite [27,28]. Oftentimes, the DSC phase transformations peaks overlap, obscuring the endset of the first peak with the onset of the second peak. Occasionally, the peaks are so close together it is difficult to even determine what the R-phase peak temperature is. Additionally, some NiTi alloys experience multi-stage martensite to austenite transformastion due to precipitate formations. In these cases the bulk material transforms first, while the material immediately surrounding the precipitates transforms later, due to internal stresses or compositional gradients that arise near the precipitate formations [29–31]. This may also result in overlapping transformation peaks that create difficulty in properly characterizing the material.

The first step in deconvoluting the peaks is to estimate the shape of the taller of the two peaks. The initial value for σ_1 must be estimated,

Table 3
Transformation characteristics determined from standard analysis.

	Rs (°C)	Rp (°C)	Rf (°C)	As (°C)	Ap (°C)	Af (°C)	Peak 1 Area J/g	Peak 2 Area J/g	Total Area J/g
TPW	27.7	–	–	49.3	58.2	62.0	–	–	14.7
SBM	−21.4	–	–	−2.4	6.3	14.1	–	–	13.3

Table 4
Transformation characteristics determined after deconvolution.

	Rs (°C)	Rp (°C)	Rf (°C)	As (°C)	Ap (°C)	Af (°C)	Peak 1 Area J/g	Peak 2 Area J/g	Total Area J/g
TPW	26.3	44.5	54.0	48.6	58.2	62.4	8.3	5.8	14.1
SBM	−26.1	−2.8	8.0	−3.9	6.3	13.6	9.2	3.8	13.0

since it cannot be determined accurately from the data. The values for n_1 and m_2 are initially set to 1. Once the shape of the taller peak has been estimated, it is subtracted from the baseline data, as shown in Fig. 3. After this subtraction, one major peak remains in the data, representing the other phase transition. This peak is approximated as best as possible by the method previously described for single peaks. This peak is then subtracted from the original baseline data set to better determine the shape of the first peak. This process is iterated several times to achieve the best curve fit for both peaks.

Fig. 4 shows how well this process fits two overlapping NiTi DSC transformation peaks. For this study, it is assumed that these materials undergo an intermediary R-phase transformation. Comparison of the characteristic transformation temperatures before and after deconvolution is presented in Tables 3 and 4. All of the characteristic temperatures determined by the deconvolution method are in good agreement with the temperatures that were ascertained from the raw data (within 1.5 °C). The only exception is the R-phase start (Rs) for the BMS sample, which was off by almost 5 °C. This discrepancy is most likely due to the inaccuracy of determining the inflection point of this shoulder peak, which has such a high degree of overlap that it is difficult for the untrained eye to even detect its presence; it appears slightly more prominently in Fig. 5. It should be noted that the R-phase peak (Rp) and R-phase finish (Rf) temperatures cannot be determined without performing a deconvolution of the peaks, which is the added benefit of performing this analysis.

The DSC analysis can become even more complicated when the

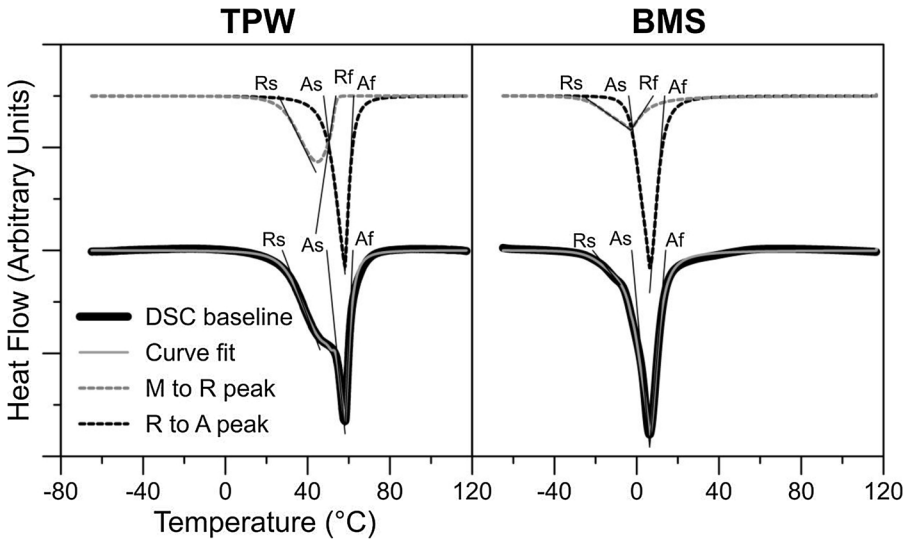

Fig. 4. Depiction of curve fitting the DSC data for the TPW and BMS samples.

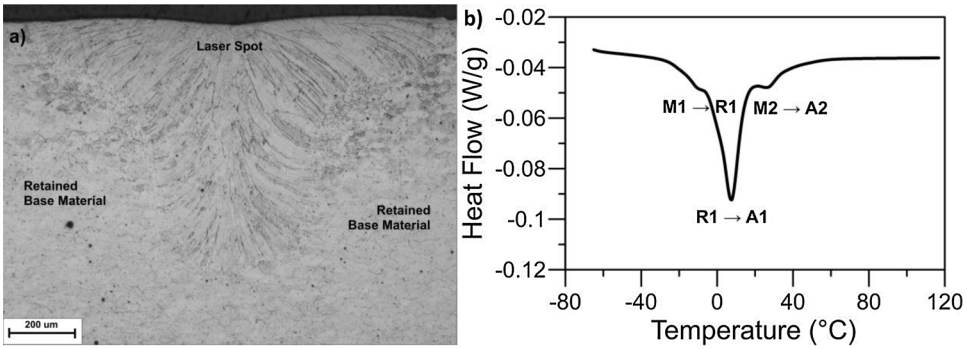

Fig. 5. a) Cross section showing the partially laser processed PS sample, and b) DSC heating curve of the PS material showing the overlapping phase transformations.

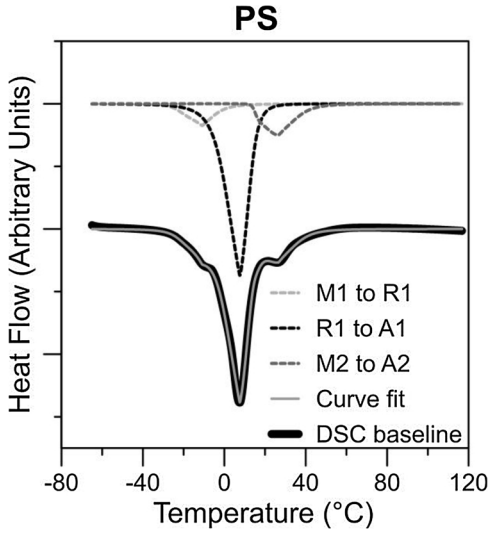

Fig. 6. Depiction of curve fitting the DSC data for the PS sample with three overlapping peaks.

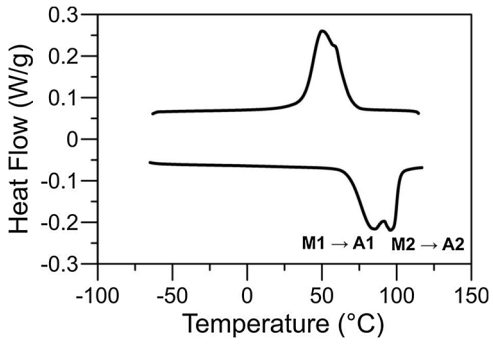

Fig. 7. DSC heating/cooling curves of the PW2 showing the overlapping transformation peaks of to segregated compositions.

material has been partially treated with a laser. Fig. 5a shows a cross-section of a NiTi sheet that has been partly remelted by a laser pulse. The remelted region experienced Ni depletion during laser processing, which changed the local composition and thus the phase transformation temperature in the region [21]. If the base material undergoes an intermediate R-phase transformation (as is assumed in this case) and the laser treated region has a slightly shifted transformation temperature, then it is possible to have three overlapping transformation peaks, as shown in Fig. 5b.

Deconvolution of three overlapping peaks proceeds in a similar manner as for two overlapping peaks. The shape of the tallest peak is estimated then subtracted, followed by the second tallest, then the shortest. Fig. 6 demonstrates the ability of this method to deconvolute three overlapping NiTi DSC transformation peaks. By this method, it would be possible to deconvolute any number of peaks for a complex nonhomogeneous NiTi shape memory alloy.

4.2. Single phase transformation with mixed compositions

When laser welding to join NiTi or laser treating to modify the composition, it is possible to get compositional segregation during solidification [21,25], as shown in Fig. 7. It is known that both phase transformations are martensite to austenite due to the hysteresis between the heating and cooling peaks. The first transformation has a hysteresis of 36 °C and the second transformation has a hysteresis of approximately 37 °C. These are typical for a martensite to austenite transformation [32]; however, the R-phase to austenite transformation has a much smaller hysteresis, typically only a few degrees [12,18]. Therefore, the material must be experiencing two separate martensite to austenite phase transformations due to the presence of two different compositions.

Even though the DSC peaks are overlapping, they can be deconvoluted by the method described previously. In addition to determining the transformation properties of each composition, the areas under the individual curves can be used to approximate the volume fraction of each composition and determine the overall bulk composition, as shown in Fig. 8. Since both compositions has similar transformation pathways (i.e. martensite directly to austenite with no intermediate phases), the ratio of the amount of energy required for each phase transformation should be approximately proportional to the ratio of the volume of each composition. In this case, the first transformation

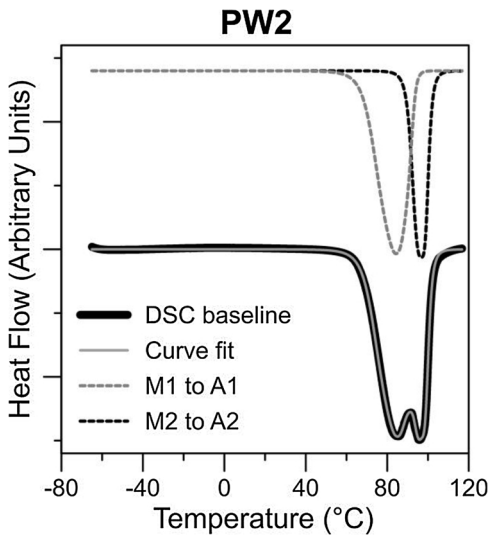

Fig. 8. Depiction of curve fitting of sample PW2 with mixed composition.

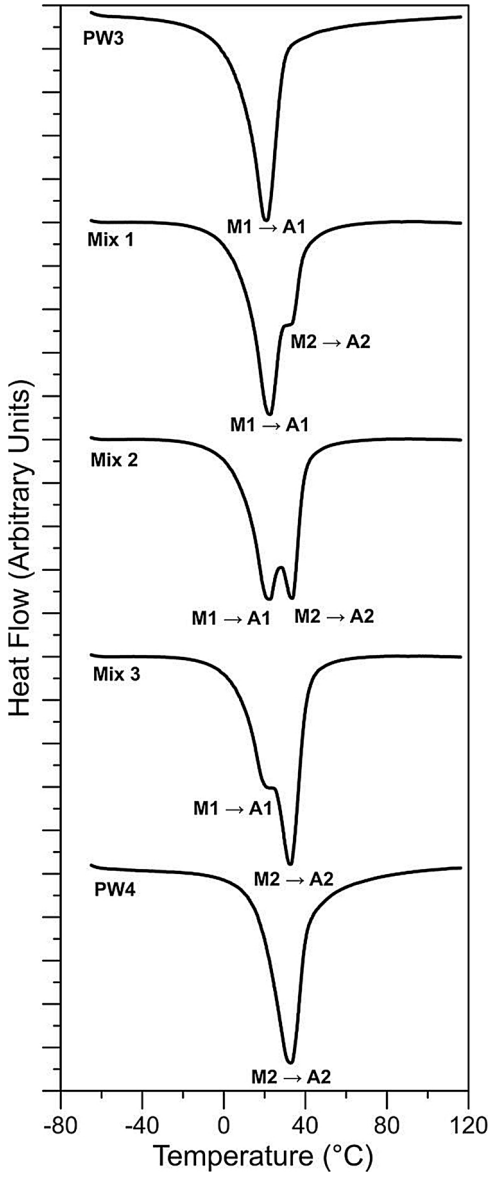

Fig. 9. DSC heating curves for PW3, PW4 and mixed samples.

volume in 55.8% of the total volume and the second transformation volume is 44.5% of the total volume.

In order to verify this method, two materials (PW3 and PW4) with known compositions and only a single transformation peak each were placed together in known quantities and analysed by DSC in three different ratios, as shown in Fig. 9. The individual peaks for PW3 and PW4 were found to have areas of 19.1 J/g and 19.5 J/g, respectively. Since both materials have similar thermomechanical histories and transformation kinetics, the overlapping DSC data can be deconvoluted and the ratio of the areas of the deconvoluted peaks can analysed and compared to the actual ratio of volumes for each material present. In all cases, the calculated volume percentage was in close agreement with the actual volume percentage (see Table 5). Additionally, the transformation temperatures of Mix 1, Mix 2 and Mix 3, which were determined through the proposed deconvolution method, are in good agreement with the actual transformation temperatures of PW3 and PW4, which were determined using the Trios software. This indicates that this method is a reasonable approximation for determining the relative volumes present for a sample with mixed compositions when both compositions have a similar microstructure and phase transformation pathway.

Table 5
List of physical volume percentages, calculated volume percentages and transformation peaks.

	Actual Volume (%)		Calculated Volume (%)		1st peak (°C)	2nd peak (°C)
PW3	100	0	100	0	20.9	N/A
Mix 1	65.8	34.2	67.8	32.2	21.7	33.7
Mix 2	51.9	48.1	53.0	47.0	20.6	33.8
Mix 3	36.9	63.1	35.1	64.9	19.8	32.7
PW4	0	100	0	100	N/A	32.7

5. Conclusions

The current work proposes an adaptive function, capable of fitting the DSC transformation curve of any shape for NiTi alloys. A method was successfully demonstrated to be able to deconvolute overlapping DSC peaks for NiTi alloys that exhibit complex phase transformation pathways. A good correlation between the newly proposed methodology and the currently used analysis techniques was established. This sets the groundwork for better material characterization of complex and non-homogeneous NiTi SMAs that implement gradient compositions or microstructures.

Acknowledgements

The authors would like to acknowledge the financial support of the Canadian Foundation for Innovation (CFI, www.innovation.ca) and the Natural Sciences and Engineering Research Council of Canada (NSERC, www.nserc.ca). The expertise and technical support of Smarter Alloys Inc. (smarteralloys.com) and the Microwelding group of the Centre for Advanced Materials Joining (CAMJ, mme.uwaterloo.ca/~camj/) were also essential to the completion of this study.

References

[1] J.A. Shaw, C.B. Churchill, M.A. Iadicola, Tip and tricks for characterizing shape memory alloy wire: part 1—differential scanning calorimetry and basic phenomena, Exp. Tech. 32 (2008) 55–62.
[2] T.G. Bradley, W.A. Brantley, B.M. Culbertson, Differential scanning calorimetry (DSC) analyses of superelastic and nonsuperelastic nickel-titanium orthodontic wires, Am. J. Orthod. Dentofac. Orthop. 109 (1996) 589–597.
[3] ASTM F2004-16 Standard Test Method for Transformation Temperature of Nickel-Titanium Alloys by Thermal Analysis, ASTM International, West Conshohocken, PA, 2016.
[4] H. Matsumoto, Characterization of NiTi phase by differential scanning calorimetry thermogram, J. Mat. Sci. Lett. 11 (1992) 588–589.
[5] K. Goubaa, M. Masse, G. Bouquet, Detection of the R-phase in Ni-Ti shape memory alloys, J. Phys. IV Colloq. 01 (1991) C4-361–C4-366.
[6] V. Antonucci, G. Faiella, M. Giordano, F. Mennella, L. Nicolais, Electrical resistivity study and characterization during NiTi phase transformation, Thermochim. Acta 462 (2007) 64–69.
[7] S. Miyazaki, K. Otsuka, Deformation and transition behavior associated with R-phase in Ti-Ni alloys, Metall. Trans. A 17 (1986) 53–63.
[8] N.A. Obaisi, M.T.S. Galang-Boquiren, C.A. Evans, T.G.P. Tsay, G. Viana, D. Berzins, S. Megremis, Comparison of the transformation temperatures of heat-activated nickel-titanium orthodontic archwires by two different techniques, Dent. Mater. 32 (2016) 879–888.
[9] N.A. Obaisi, M.T.S. Galang, C.A. Evans, T.P. Tsay, M.G. Viana, H. Lukic, S. Megremis, Determination of transformation-temperature-ranges of orthodontic nickel-titanium-archwires using the bend-and-free-recovery test, Seattle, Washington, USA, March 20–23, Proceedings of IADR/AADR/CADR General Session and Exhibition 2013 (2013).
[10] ASTM F2082/F2082M-16 Standard Test Method for Determination of Transformation Temperature of Nickel-Titanium Shape Memory Alloys by Bend and Free Recovery, ASTM International, West Conshohocken, PA, 2016.
[11] J. Khalili-Allafi, B. Amin-Ahmadi, The effect of composition on enthalpy and entropy changes of martensitic transformations in binary shape memory alloys, J. Alloys Compd. 487 (2009) 363–366.
[12] Y. Zhou, J. Zhang, G. Fan, X. Ding, J. Sun, X. Ren, K. Otsuka, Origin of 2-stage R-phase transformation in low-temperature aged Ni-rich Ti-Ni alloys, Acta Mater. 53 (2005) 5365–5377.
[13] J.I. Kim, Y. Liu, S. Miyazaki, Ageing-induced two-stage R-phase transformation in Ti-50.9 at%Ni, Acta Mater. 52 (2004) 487–499.
[14] C. Sandu, R.K. Singh, Modeling differential scanning calorimetry, Thermochim.

Acta 159 (1990) 267–298.
[15] X. Shi, L. Cui, D. Jiang, C. Yu, F. Guo, M. Yu, Y. Ren, Y. Liu, Grain size effect on the R-phase transformation of nanocrystalline NiTi shape memory alloys, J. Mater. Sci. 49 (2014) 4643–4647.
[16] Y. Monetmani, M. Nili-Ahmadabadi, T.J. Tan, M. Bornapour, S. Rayagan, Effect of cooling rate on the phase transformation behavior and mechanical properties of Ni-rich NiTi shape memory alloy, J. Alloys Compd. 469 (2009) 164–168.
[17] Y. Zheng, F. Jiang, L. Li, H. Yang, Y. Liu, Effect of ageing treatment on the transformation behavior of Ti-50.9 at.% Ni alloy, Acta Mater. 56 (2008) 736–745.
[18] G. Fan, W. Chen, S. Yang, J. Zhu, X. Ren, K. Otsuka, Origin of abnormal multi-stage martensitic transformation behavior in aged Ni-rich Ti-Ni shape memory alloys, Acta Mater. 52 (2004) 4351–4362.
[19] W. Tang, Thermodynamic study of the low-temperature phase, B19' and martensitic transformation in near equiatomic Ti-Ni shape memory alloys, Metall. Mater. Trans. A 28 (1997) 537.
[20] J. Frenzel, E.P. George, A. Dlouhy, C. Somsen, M.F.-X. Wagner, G. Eggeler, Influence of Ni on martensitic phase transformations in NiTi shape memory alloys, Acta Mater. 58 (2010) 3444–3458.
[21] M.I. Khan, A. Pequegnat, Y.N. Zhou, Multiple memory shape memory alloys, Adv. Eng. Mater. 15 (2013) 386–393.
[22] C.P. Frick, A.M. Ortega, J. Tyber, A.El.M. Maksound, H.J. Maier, Y. Liu, K. Gall, Thermal processing of polycrystalline NiTi shape memory alloys, Mater. Sci. Eng.: A 405 (2005) 34–49.
[23] A. Pequegnat, B. Panton, Y.N. Zhou, M.I. Khan, Local composition and microstructural control for multiple pseudoelastic plateaus and hybrid self-biasing shape memory alloys, Mater. Des. 92 (2016) 802–813.
[24] A. Michael, Y.N. Zhou, M.I. Khan, Experimental validation of a one-dimensional model for monolithic shape memory alloys with multiple pseudoelastic plateaus, J. Intell. Mater. Syst. Struct. 27 (2016) 2102–2111.
[25] B. Panton, A. Michael, Y.N. Zhou, M.I. Khan, Effects of post-processing on the thermomechanical fatigue properties of laser modified NiTi, Int. J. Fatigue (2018), http://dx.doi.org/10.1016/j.ijfatigue.2017.11.012 (in press).
[26] T. Waitz, T. Antretter, F.D. Fischer, H.P. Karnthaler, Size effects on the martensitic phase transformations in nanocrystalline NiTi shape memory alloys, Mater. Sci. Technol. 24 (2008) 934–940.
[27] N.A. Zarkevich, D.D. Johnson, Shape-memory transformations of NiTi: minimum-energy pathways between austenite, martensites, and kinetically limited intermediate states, Phys. Rev. Lett. 113 (2014) 256701-1–265701-5.
[28] T.W. Duerig, K. Bhattacharya, The influence of the R-phase on the superelastic behavior of NiTi, Shape Mem. Superelastic. 1 (2015) 153–161.
[29] J. Khalil Allafi, X. Ren, G. Eggeler, The mechanism of multistage transformations in aged Ni-rich NiTi shape memory alloys, Acta Mater. 50 (2002) 793–803.
[30] J. Khalil-Allafi, A. Dlouhy, G. Eggeler, Ni_4Ti_3-precipitation during aging of NiTi shape memory alloys and its influence on martensitic phase transformations, Acta Mater. 50 (2002) 4255–4272.
[31] J. Michutta, Ch. Somsen, A. Yawny, A. Dlouhy, G. Eggeler, Elementary martensitic transformation processes in Ni-rich NiTi single crystals with Ni_4Ti_3 precipitates, Acta Mater. 54 (2006) 3525–3542.
[32] R.F. Hamilton, H. Sehitoglu, Y. Chumlyakov, H.J. Maier, Stress dependence of the hysteresis in single crystal NiTi alloys, Acta Mater. 52 (2004) 3383–3402.